Δ^{++} production in hadronic Z^0 decays

The OPAL Collaboration

Abstract

The production of Δ^{++} baryons has been measured using 3.5 million hadronic Z^0 decays collected with the OPAL detector at LEP. The production rate and fragmentation function are presented. A total of $0.22 \pm 0.04 \pm 0.04$ $\Delta^{++} + (\overline{\Delta})^{--}$ per hadronic Z^0 decay is observed. The fragmentation function is found to be softer than that predicted by the JETSET and HERWIG Monte Carlo event generators. With this measurement of Δ^{++} production, at least one baryon of each strangeness level in the lightest baryon decuplet has now been measured at LEP.

(Submitted to Physics Letters B)

The OPAL Collaboration

G. Alexander[23], J. Allison[16], N. Altekamp[5], K. Ametewee[25], K.J. Anderson[9], S. Anderson[12],
S. Arcelli[2], S. Asai[24], D. Axen[29], G. Azuelos[18,a], A.H. Ball[17], E. Barberio[26], R.J. Barlow[16],
R. Bartoldus[3], J.R. Batley[5], G. Beaudoin[18], J. Bechtluft[14], A. Beck[23], G.A. Beck[13],
C. Beeston[16], T. Behnke[8], K.W. Bell[20], G. Bella[23], S. Bentvelsen[8], P. Berlich[10], S. Bethke[14],
O. Biebel[14], I.J. Bloodworth[1], P. Bock[11], H.M. Bosch[11], M. Boutemeur[18], S. Braibant[12],
P. Bright-Thomas[25], R.M. Brown[20], H.J. Burckhart[8], C. Burgard[27], R. Bürgin[10], P. Capiluppi[2],
R.K. Carnegie[6], A.A. Carter[13], J.R. Carter[5], C.Y. Chang[17], C. Charlesworth[6], D.G. Charlton[1,b],
S.L. Chu[4], P.E.L. Clarke[15], J.C. Clayton[1], S.G. Clowes[16], I. Cohen[23], J.E. Conboy[15],
O.C. Cooke[16], M. Cuffiani[2], S. Dado[22], C. Dallapiccola[17], G.M. Dallavalle[2], C. Darling[31], S. De
Jong[12], L.A. del Pozo[8], H. Deng[17], M.S. Dixit[7], E. do Couto e Silva[12], E. Duchovni[26],
G. Duckeck[8], I.P. Duerdoth[16], U.C. Dunwoody[8], J.E.G. Edwards[16], P.G. Estabrooks[6],
H.G. Evans[9], F. Fabbri[2], B. Fabbro[21], P. Fath[11], F. Fiedler[12], M. Fierro[2], M. Fincke-Keeler[28],
H.M. Fischer[3], R. Folman[26], D.G. Fong[17], M. Foucher[17], H. Fukui[24], A. Fürtjes[8], P. Gagnon[6],
A. Gaidot[21], J.W. Gary[4], J. Gascon[18], S.M. Gascon-Shotkin[17], N.I. Geddes[20], C. Geich-Gimbel[3],
S.W. Gensler[9], F.X. Gentit[21], T. Geralis[20], G. Giacomelli[2], P. Giacomelli[4], R. Giacomelli[2],
V. Gibson[5], W.R. Gibson[13], J.D. Gillies[20], D.M. Gingrich[30,a], J. Goldberg[22], M.J. Goodrick[5],
W. Gorn[4], C. Grandi[2], E. Gross[26], C. Hajdu[32], G.G. Hanson[12], M. Hansroul[8], M. Hapke[13],
C.K. Hargrove[7], P.A. Hart[9], C. Hartmann[3], M. Hauschild[8], C.M. Hawkes[8], R. Hawkings[8],
R.J. Hemingway[6], G. Herten[10], R.D. Heuer[8], J.C. Hill[5], S.J. Hillier[8], T. Hilse[10], P.R. Hobson[25],
D. Hochman[26], R.J. Homer[1], A.K. Honma[28,a], D. Horváth[32,c], R. Howard[29],
R.E. Hughes-Jones[16], D.E. Hutchcroft[5], P. Igo-Kemenes[11], D.C. Imrie[25], A. Jawahery[17],
P.W. Jeffreys[20], H. Jeremie[18], M. Jimack[1], A. Joly[18], M. Jones[6], R.W.L. Jones[8], U. Jost[11],
P. Jovanovic[1], J. Kanzaki[24], D. Karlen[6], K. Kawagoe[24], T. Kawamoto[24], R.K. Keeler[28],
R.G. Kellogg[17], B.W. Kennedy[20], B.J. King[8], J. King[13], J. Kirk[29], S. Kluth[5], T. Kobayashi[24],
M. Kobel[10], D.S. Koetke[6], T.P. Kokott[3], S. Komamiya[24], R. Kowalewski[8], T. Kress[11],
P. Krieger[6], J. von Krogh[11], P. Kyberd[13], G.D. Lafferty[16], H. Lafoux[21], R. Lahmann[17],
W.P. Lai[19], D. Lanske[14], J. Lauber[15], J.G. Layter[4], A.M. Lee[31], E. Lefebvre[18], D. Lellouch[26],
J. Letts[2], L. Levinson[26], C. Lewis[15], S.L. Lloyd[13], F.K. Loebinger[16], G.D. Long[17], B. Lorazo[18],
M.J. Losty[7], J. Ludwig[10], A. Luig[10], A. Malik[21], M. Mannelli[8], S. Marcellini[2], C. Markus[3],
A.J. Martin[13], J.P. Martin[18], G. Martinez[17], T. Mashimo[24], W. Matthews[25], P. Mättig[3],
J. McKenna[29], E.A. Mckigney[15], T.J. McMahon[1], A.I. McNab[13], F. Meijers[8], S. Menke[3],
F.S. Merritt[9], H. Mes[7], J. Meyer[27], A. Michelini[8], G. Mikenberg[26], D.J. Miller[15], R. Mir[26],
W. Mohr[10], A. Montanari[2], T. Mori[24], M. Morii[24], U. Müller[3], B. Nellen[3], B. Nijjhar[16],
S.W. O'Neale[1], F.G. Oakham[7], F. Odorici[2], H.O. Ogren[12], N.J. Oldershaw[16], C.J. Oram[28,a],
M.J. Oreglia[9], S. Orito[24], M. Palazzo[2], J. Pálinkás[33], J.P. Pansart[21], J.R. Pater[16],
G.N. Patrick[20], M.J. Pearce[1], P.D. Phillips[16], J.E. Pilcher[9], J. Pinfold[30], D.E. Plane[8],
P. Poffenberger[28], B. Poli[2], A. Posthaus[3], T.W. Pritchard[13], H. Przysiezniak[30], D.L. Rees[1],
D. Rigby[1], M.G. Rison[5], S.A. Robins[13], N. Rodning[30], J.M. Roney[28], E. Ros[8], A.M. Rossi[2],
M. Rosvick[28], P. Routenburg[30], Y. Rozen[8], K. Runge[10], O. Runolfsson[8], D.R. Rust[12],
R. Rylko[25], M. Sasaki[24], C. Sbarra[2], A.D. Schaile[8], O. Schaile[10], F. Scharf[3], P. Scharff-Hansen[8],
P. Schenk[4], B. Schmitt[3], M. Schröder[8], H.C. Schultz-Coulon[10], M. Schulz[8], P. Schütz[3],
J. Schwiening[3], W.G. Scott[20], M. Settles[12], T.G. Shears[16], B.C. Shen[4],
C.H. Shepherd-Themistocleous[7], P. Sherwood[15], G.P. Siroli[2], A. Sittler[27], A. Skillman[15],
A. Skuja[17], A.M. Smith[8], T.J. Smith[28], G.A. Snow[17], R. Sobie[28], S. Söldner-Rembold[10],

R. W. Springer[30], M. Sproston[20], A. Stahl[3], M. Starks[12], C. Stegmann[10], K. Stephens[16], J. Steuerer[28], B. Stockhausen[3], D. Strom[19], F. Strumia[8], P. Szymanski[20], R. Tafirout[18], P. Taras[18], S. Tarem[26], M. Tecchio[8], N. Tesch[3], M.A. Thomson[8], E. von Törne[3], S. Towers[6], M. Tscheulin[10], T. Tsukamoto[24], E. Tsur[23], A.S. Turcot[9], M.F. Turner-Watson[8], P. Utzat[11], R. Van Kooten[12], G. Vasseur[21], P. Vikas[18], M. Vincter[28], E.H. Vokurka[16], F. Wäckerle[10], A. Wagner[27], D.L. Wagner[9], C.P. Ward[5], D.R. Ward[5], J.J. Ward[15], P.M. Watkins[1], A.T. Watson[1], N.K. Watson[7], P. Weber[6], P.S. Wells[8], N. Wermes[3], B. Wilkens[10], G.W. Wilson[27], J.A. Wilson[1], T. Wlodek[26], G. Wolf[26], S. Wotton[11], T.R. Wyatt[16], S. Xella[2], G. Yekutieli[26], V. Zacek[18],

[1]School of Physics and Space Research, University of Birmingham, Birmingham B15 2TT, UK

[2]Dipartimento di Fisica dell' Università di Bologna and INFN, I-40126 Bologna, Italy

[3]Physikalisches Institut, Universität Bonn, D-53115 Bonn, Germany

[4]Department of Physics, University of California, Riverside CA 92521, USA

[5]Cavendish Laboratory, Cambridge CB3 0HE, UK

[6] Ottawa-Carleton Institute for Physics, Department of Physics, Carleton University, Ottawa, Ontario K1S 5B6, Canada

[7]Centre for Research in Particle Physics, Carleton University, Ottawa, Ontario K1S 5B6, Canada

[8]CERN, European Organisation for Particle Physics, CH-1211 Geneva 23, Switzerland

[9]Enrico Fermi Institute and Department of Physics, University of Chicago, Chicago IL 60637, USA

[10]Fakultät für Physik, Albert Ludwigs Universität, D-79104 Freiburg, Germany

[11]Physikalisches Institut, Universität Heidelberg, D-69120 Heidelberg, Germany

[12]Indiana University, Department of Physics, Swain Hall West 117, Bloomington IN 47405, USA

[13]Queen Mary and Westfield College, University of London, London E1 4NS, UK

[14]Technische Hochschule Aachen, III Physikalisches Institut, Sommerfeldstrasse 26-28, D-52056 Aachen, Germany

[15]University College London, London WC1E 6BT, UK

[16]Department of Physics, Schuster Laboratory, The University, Manchester M13 9PL, UK

[17]Department of Physics, University of Maryland, College Park, MD 20742, USA

[18]Laboratoire de Physique Nucléaire, Université de Montréal, Montréal, Quebec H3C 3J7, Canada

[19]University of Oregon, Department of Physics, Eugene OR 97403, USA

[20]Rutherford Appleton Laboratory, Chilton, Didcot, Oxfordshire OX11 0QX, UK

[21]CEA, DAPNIA/SPP, CE-Saclay, F-91191 Gif-sur-Yvette, France

[22]Department of Physics, Technion-Israel Institute of Technology, Haifa 32000, Israel

[23]Department of Physics and Astronomy, Tel Aviv University, Tel Aviv 69978, Israel

[24]International Centre for Elementary Particle Physics and Department of Physics, University of Tokyo, Tokyo 113, and Kobe University, Kobe 657, Japan

[25]Brunel University, Uxbridge, Middlesex UB8 3PH, UK

[26]Particle Physics Department, Weizmann Institute of Science, Rehovot 76100, Israel

[27]Universität Hamburg/DESY, II Institut für Experimental Physik, Notkestrasse 85, D-22607 Hamburg, Germany

[28]University of Victoria, Department of Physics, P O Box 3055, Victoria BC V8W 3P6, Canada

[29]University of British Columbia, Department of Physics, Vancouver BC V6T 1Z1, Canada
[30]University of Alberta, Department of Physics, Edmonton AB T6G 2J1, Canada
[31]Duke University, Dept of Physics, Durham, NC 27708-0305, USA
[32]Research Institute for Particle and Nuclear Physics, H-1525 Budapest, P O Box 49, Hungary
[33]Institute of Nuclear Research, H-4001 Debrecen, P O Box 51, Hungary

[a]Also at TRIUMF, Vancouver, Canada V6T 2A3
[b] Royal Society University Research Fellow
[c] Institute of Nuclear Research, Debrecen, Hungary

1 Introduction

Various measurements of inclusive baryon rates and fragmentation functions have been made in hadronic Z^0 decays [1, 2, 3, 4]. These measurements provide insight into the process by which quarks and gluons become confined inside hadrons, known as fragmentation, and allow models for fragmentation to be tested. The best probes of the fragmentation process are particles which are produced directly in the fragmentation process and only rarely as decay products ("direct production"). In this sense the $J^P = \frac{3}{2}^+$ decuplet baryons are good probes of the fragmentation process. In hadronic Z^0 decays there have been measurements of the Ω^- (strangeness, S = -3), the $\Xi(1530)^0$ (S = -2) and the $\Sigma(1385)^\pm$ (S = -1) [1, 3]. Only a measurement of the S = 0, $\Delta(1232)$, is still missing.

Of the possible charged states of the Δ, the Δ^{++} is the easiest to measure in e^+e^- collisions, due to its 100% branching ratio to charged particles. The Δ^{++} has a mass of 1.232 GeV/c^2, a width of approximately 110 MeV/c^2, and decays strongly to $p\pi^+$ with a branching ratio of 100% [5]. Since the Δ^{++} mass is near the $p\pi^+$ threshold, the signal tends to be accompanied by a rising combinatorial background. This background easily obscures the wide Δ^{++} signal and thus it is imperative to understand the background shapes under the Δ^{++} signal to be able to make a reliable measurement of the production rate.

The Δ^{++} has been observed only once before in e^+e^- collisions, when a measurement was made near the $\Upsilon(1S)$ resonance and in the nearby continuum [6]. The fragmentation function was reported only at the $\Upsilon(1S)$.

This letter reports the first observation of Δ^{++} production[1] at centre-of-mass energies $\sqrt{s} \approx 91$ GeV together with a measurement of the Δ^{++} fragmentation function. The measurement was made with the OPAL detector using data collected at the LEP electron positron collider at CERN during the 1990–1994 running periods. This data sample corresponds to approximately 3.5 million hadronic Z^0 decays.

2 The OPAL Detector

The OPAL detector has been described in detail elsewhere [7]. Relevant to this analysis is the tracking system, in particular three sets of drift chambers, an inner vertex chamber, a jet chamber, and a system of chambers that precisely measures the z coordinate of tracks at polar angles[2] less than $|\cos(\theta)| < 0.72$ (z-chambers). The tracking system is in an axial magnetic field of 0.435 T. The jet chamber has 159 signal wires per 15° ϕ sector and provides a measurement of the specific ionisation energy loss (dE/dx) of charged particles in the chamber gas [8]. Outside the magnet coil, in the polar angle range $|\cos(\theta)| < 0.72$, there is a system of time-of-flight (TOF) counters.

---

[1]Throughout this letter, unless explicitly stated otherwise, we use the baryon, Δ^{++}, to imply the sum of the baryon and the anti-baryon, $(\overline{\Delta})^{--}$.

[2]The OPAL coordinate system is right handed and defined such that the z axis follows the electron beam direction and the x axis points in the direction of the centre of the LEP ring. The polar and azimuthal angles, θ and ϕ, are defined with respect to the z and x axes, respectively.

3 Δ^{++} Selection

Hadronic decays of the Z^0 were selected as in [9]. Since the Δ^{++} decays strongly to $p\pi^+$, the decay products originate from the event vertex. For each event the primary vertex was found, using the method of [10] without the beam constraint, and only charged tracks assigned to the event vertex were used. To provide a good measurement of the particle dE/dx, these tracks were required to have at least 30 dE/dx samples used in the calculation of the energy loss.

The proton selection was designed to provide as good as possible rejection of pions and kaons, so as to reduce sensitivity to the $\pi^+\pi^+$ and $K^+\pi^+$ backgrounds. In particular, the $K^+\pi^+$ background is troublesome as it tends to peak very close to the Δ^{++} mass. Tracks were considered as proton candidates if they were within $|\cos(\theta)| < 0.72$, had a polar angle measurement in the z-chambers, and if the particle identification probabilities, calculated from the dE/dx measurement, were such that the proton probability was greater than 50%, and the pion and kaon probabilities were less than 40%. Additionally, if the proton candidate was in the momentum range $1.2 < p < 2.0$ GeV/c and a measurement of the time-of-flight was made in the TOF counters, it was rejected if the measured time-of-flight gave a probability of greater than 40% for the particle to be a pion. This requirement is made in the momentum region where the pion and proton dE/dx separation is ambiguous, in order to reject pions that would otherwise overwhelm the signal.

Any track that was assigned to the primary vertex and satisfied the requirement on the number of dE/dx samples was considered to be a pion candidate if it had a polar angle measurement in the z-chambers or it exited through the ends of the jet chamber. For the tracks passing through the ends of the jet chamber (roughly $|\cos(\theta)| > 0.74$), the end of the last wire which registered a hit in the jet chamber was taken to be the point at which the track exited from the chamber. The measurement of $\cos(\theta)$ is significantly improved by using this endpoint information.

The above proton and pion candidates were combined to form $p\pi^+$ candidate pairs with the requirement that the proton momentum be greater than the pion momentum ($p_p > p_{\pi^+}$). The $p\pi^+$ candidates were binned in six intervals of the scaled energy, $x_E = E_{p\pi^+}/E_{\text{beam}}$. The resulting invariant mass spectra are shown in figure 1. In figure 1 one sees a set of distributions that rise quickly from threshold, exhibit broad peaks around 1.2 GeV/c^2, and then slowly fall towards higher masses. As will be explained later, the gross features of these distributions are due to background processes which vary from one x_E bin to the next. Since these backgrounds peak in the mass range where a Δ^{++} signal is expected, it is necessary to have a solid understanding of these processes.

4 Efficiency Determination

The efficiency for the tracks from Δ^{++} decay to be used in the primary vertex fit, to be in the angular acceptance, and to have $p_p > p_{\pi^+}$ was calculated using a Monte Carlo simulation. This Monte Carlo sample consisted of two million JETSET 7.3 [11] events that were passed through a simulation of the OPAL detector [12] and reconstructed in the same way as the data. The remaining selection efficiencies were determined from the data.

The efficiency for having 30 dE/dx samples and a polar angle measurement provided by the z-chambers or the jet chamber endpoint was determined from the set of all data tracks that were used in the primary vertex fit. These tracks were grouped into bins of momentum and $|\cos(\theta)|$ and the efficiency for these requirements was determined. In the Monte Carlo, pions

and protons from Δ^{++} decay have a slightly higher efficiency for these requirements than an average of tracks which are associated to the primary vertex. This is due to the inclusion of tracks in the vertex fit that do not originate from the event vertex. To compensate for this effect, which on average amounts to a 5% relative shift in the efficiency, the fractional difference between all tracks and the tracks from Δ^{++} decay in the Monte Carlo was found and the data efficiencies were scaled by this relative difference. Half of the correction was added to the estimated error in the efficiency.

The proton identification efficiency was determined using protons from $\Lambda \to p\pi^-$ decays. Candidates for Λ decays were found using the second method described in [1], without proton identification requirements and with the signal region defined as $1.112 < m_{p\pi^-} < 1.120 \text{ GeV}/c^2$. Since the proton identification efficiency for tracks originating at the event vertex was required, only Λ candidates with a reconstructed radius of the decay point of less than 20 cm were used. The proton from the Λ decay was required to satisfy all the Δ^{++} track requirements (except the primary vertex requirement). The $p\pi^-$ invariant mass plots were fitted to determine the amount of background in the signal region, before and after the proton identification requirements were applied. The efficiency was determined as the probability for a Λ to survive the proton selection requirements in bins of the proton momentum.

Applying the track selection requirements in the Monte Carlo results in predictions for the momenta and $|\cos(\theta)|$ spectra for the Δ^{++} decay products in bins of x_E. The efficiencies derived from data (in momentum and $|\cos(\theta)|$) were applied to these spectra to obtain the final Δ^{++} selection efficiencies. These efficiencies are given in table 1.

5   Fitting the Invariant Mass Spectra

As can be seen in figure 1, the $p\pi^+$ candidate invariant mass shapes vary substantially with x_E. The majority of the candidates are backgrounds, either non-Δ^{++} $p\pi^+$ pairs or pairs with one or both of the proton and pion candidates misidentified. In the region $0.075 < x_E < 0.1$ the background is mostly $\pi^+\pi^+$, the shape of the resulting invariant mass distribution being due to the proton selection criteria in the region where the dE/dx particle identification becomes ambiguous. One π^+ is identified as a proton and this biases the $\pi^+\pi^+$ distribution to higher masses. Fitting a simple background shape could easily hide any peaking structures in the background components. Since the background shapes are seen to vary with x_E, fitting the sum of all x_E bins hides some of the structure in the background and could possibly bias the Δ^{++} production rate determination if the fragmentation functions for charged particles are not simulated correctly in the Monte Carlo.

The invariant mass spectra were fitted, using a χ^2 minimisation method, to the sum of a Breit-Wigner shape for the Δ^{++} signal and sixteen background shapes obtained from Monte Carlo simulations. The background shapes consisted of all possible two particle combinations of p, π^+, K^+, and all other possible charged tracks. Eight normalisation factors were used that determined the various particle production rate normalisations and dE/dx efficiencies. Denoting the normalisation factors as

R_{ip} the normalisation factor for particle i to be identified as a proton
$R_{j\pi^+}$ the normalisation factor for particle j to be identified as a pion

each bin of x_E was fitted to the expression

$$N(m) = R_{\Delta^{++}} \text{BW}(m) + \sum_{ij} R_{ip} R_{j\pi^+} f_{ij}^{\text{MC}}(m),$$

6

with the R factors as free parameters; $R_{\Delta^{++}}$ determines the signal normalisation. The sum over i denotes the possible proton candidate sources (p, π^+, K^+ and other) and the sum over j includes all possible sources of pion candidates. The function $f_{ij}^{\text{MC}}(m)$ denotes the Monte Carlo predicted shape for ij pairs. $\text{BW}(m)$ is the signal shape given by [13]:

$$\text{BW}(m) = \frac{m_0\Gamma(m)}{(m_0^2 - m^2)^2 + (m_0\Gamma(m))^2},$$

where m_0 is the Δ^{++} mass and the width, $\Gamma(m)$, is given by:

$$\Gamma(m,q) = \Gamma_0 \left(\frac{q}{q_0}\right)^3 \left(\frac{m_0}{m}\right)^2 \frac{(m + m_{\text{p}})^2 - m_\pi^2}{(m_0 + m_{\text{p}})^2 - m_\pi^2}.$$

Γ_0 is the Δ^{++} on-shell width, q is the momentum of the decay products in the Δ^{++} rest frame, $q = q_0$ when $m = m_0$, and m_{p} and m_π are the proton and pion masses respectively. The Δ^{++} mass resolution obtained using a simulation of the OPAL detector varies between 3 and 10 MeV/c^2, and in the fits the Breit-Wigner shape was convolved with a Gaussian of $\sigma = 5$ MeV/c^2. However, since the Δ^{++} width is much larger than this resolution, this correction makes very little difference. As expected, the fits predict that $\text{p}\pi^+$, $\pi^+\pi^+$ and $K^+\pi^+$ make up the majority of the total background.

Fitting the $\text{p}\pi^+$ candidate spectra in this way has several advantages. Fitting only eight normalisation factors enforces the correlations present in the background sources. For example, if the pion rate were incorrect in the Monte Carlo, then the $\text{p}\pi^+$ and $K^+\pi^+$ shapes would need to be scaled by the same factor, that which gives the correct π^+ rate. Also by fitting predicted shapes instead of a single smooth background shape, the fit is sensitive to any peaking structures that might be present in the background shapes.

Figure 1 shows all six bins of x_E with the fitted Δ^{++} signal and background contributions. The fitted number of Δ^{++} per event in each bin of x_E is given in table 2 along with the χ^2 probabilities for fits both with and without a Δ^{++} signal. In the x_E ranges with a significant fitted signal, the probability that there is no Δ^{++} component is small. The error from the fit includes the statistical error in both the data and the Monte Carlo background shapes. In figure 1 it should be noted that the rise and the region above 1.5 GeV/c^2, where there is very little signal, are well described by the fit. The background normalisation needed to fill in the fitted Δ^{++} signal would diminish the agreement in these regions. This point is further illustrated in figure 2, which shows the fitted $\text{p}\pi^+$, $\pi^+\pi^+$ and $\pi^+\text{p}$ background components for the x_E range 0.075–0.1. These shapes are very different from each other and none of them could be rescaled to absorb the Δ^{++} signal and maintain the good description of the rise and fall of the distribution. Figure 2d shows the data after subtraction of the fitted background along with the fitted Δ^{++} signal in this range and figure 3 shows this distribution summed over all six bins of x_E.

To check that the fit is actually sensitive to a wide resonance centred at the Δ^{++} mass, the fit was performed with the mass of the Δ^{++} free. Table 3 shows that the results of this fit are consistent with those from the fixed mass fit and the fitted mass is close to the nominal mass of 1.232 GeV/c^2.

Since the fit to the invariant mass spectrum relies on the Monte Carlo predicted background shapes, it is necessary to verify that the Monte Carlo reproduces the data shapes. It has been verified that when $\pi^+\pi^+$ and $K^+\pi^+$ are selected in the data and Monte Carlo, the Monte Carlo gives a good representation of the resulting spectra. For the case of $\pi^+\pi^+$, demanding that

7

the pion that is misidentified as a proton have larger momentum than the other pion lessens the effect of Bose-Einstein correlations. The rates of partially reconstructed decays that give $p\pi^+$ candidate masses near the Δ^{++} mass were allowed to vary in the fits and no significant differences in the Δ^{++} rate were found. An $N(1440)P_{11}$, which decays to $p\pi^+$, was added to the $p\pi^+$ spectra and no resulting change in the Δ^{++} rate was observed. The data were selected with the proton selection requirements varied by 10% and the rate determined was consistent with the stated rate. Finally the fit was performed with only the three main background sources, $p\pi^+$, $\pi^+\pi^+$, and $K^+\pi^+$, instead of the sixteen possible sources. This fit gave results consistent with the full fit. Thus the fits are stable with respect to small variations in the assumed background shapes.

6   Results and Systematic Errors

Correcting each bin for efficiency, integrating over all momentum bins and extrapolating in the unmeasured region gives a total production rate of $0.22 \pm 0.04 \pm 0.04$ Δ^{++} per hadronic Z^0 decay, where the first error is statistical and the second is systematic. The sources of systematic error considered and the extrapolation used in the unmeasured region are detailed below. As a comparison, the Monte Carlo event generator HERWIG 5.6 [14] predicts a rate of 0.17, JETSET predicts 0.18, and the model of [15] predicts 0.17, all in agreement with this measurement[3]. Table 4 gives the measured Δ^{++} fragmentation function and figure 4 shows the Δ^{++} fragmentation function together with the predicted fragmentation functions of JETSET and HERWIG. The JETSET and HERWIG predictions have been normalised to the observed rate above $x_E = 0.05$, which is $0.16 \pm 0.03 \pm 0.01$ Δ^{++} per hadronic Z^0 decay. As is the general trend for baryons at LEP, both JETSET and HERWIG predict a fragmentation function that is harder than the data.

The sources of systematic error considered were the Monte Carlo modelling of the detector for the vertex assignment criteria, the dependence of the determination of the efficiency in each x_E bin on the assumed fragmentation function, the integration of the Breit-Wigner shape, and the extrapolation below $x_E = 0.05$. The fits were found to give consistent results with respect to small variations in the dE/dx selection criteria and the number of samples used in the dE/dx calculation.

The efficiency for assigning tracks from Δ^{++} decay to the primary vertex was investigated in the Monte Carlo. The vertex assignment requirements were varied in the Monte Carlo and the efficiencies re-determined. The second column of table 5 gives the errors in the differential rate due to this uncertainty in the vertex modelling in the Monte Carlo.

The average Δ^{++} selection efficiency within each x_E bin was determined assuming the fragmentation function of JETSET. The third column of table 5 gives the change in the differential rate in each bin of x_E when the fragmentation function of HERWIG is used in determining the efficiency.

In calculating the observed number of Δ^{++} in each x_E bin, the Breit-Wigner shape was integrated only up to 1.6 GeV/c^2. When the Breit-Wigner shape was integrated up to the kinematically allowed maximum in each bin, a production rate approximately 6% higher was obtained. Since the Δ^{++} selection efficiency was evaluated only to 1.6 GeV/c^2, and since it is possible that the selection efficiency decreases with the Δ^{++} momentum, we add one half of the possible missing rate to the result and assign an error equal to the full correction. This

---

[3]The parameter values used for JETSET and HERWIG are given in [16].

error is given in the fourth column of table 5.

The region of x_E below 0.05 is dominated by background, leading to unreliable fits, hence an extrapolation is needed to determine the integrated rate. According to JETSET, 28.8% of the total rate is below $x_E = 0.05$ whereas HERWIG predicts that 29.3% of the production is below 0.05. The JETSET value was used for the extrapolation of the rate below $x_E = 0.05$. To estimate an uncertainty on this extrapolation we note that in the OPAL measurement of the inclusive proton rate [2], the Monte Carlo predictions and the measurement of the fractional rate below $x_E = 0.05$ disagree by large amounts. Thus 50% of the JETSET predicted extrapolation is added as a systematic error on the extrapolation in the unmeasured region of x_E, which amounts to an error of 0.04 on the total rate. This uncertainty in the extrapolation dominates the overall systematic error on the rate determination.

7   Discussion

The model of baryon production implemented in JETSET proceeds by string breaking into a diquark anti-diquark pair. There are parameters that control the ratio of diquark to quark creation at the string breaking, the rate of strange quark creation, both in quark and diquark production, and the ratio of spin one diquarks to spin zero diquarks. The HERWIG model proceeds by decays of clusters into known particles, with the maximum cluster mass being the main parameter which determines particle rates.

With this measurement of Δ^{++} production, at least one state of each of the strangeness levels in the lightest baryon decuplet has been measured. This makes it possible to study the strangeness suppression in this baryon decuplet. From the previous OPAL measurements of the rates of Ω^-, $\Xi(1530)^0$, and $\Sigma(1385)^+$ [1], the ratios of the production rates of particles of different strangeness are obtained

$$
\begin{aligned}
\Sigma(1385)^+/\Delta^{++} &= 0.086 \pm 0.027, \\
\Xi(1530)^0/\Delta^{++} &= 0.029 \pm 0.010, \\
\Omega^-/\Delta^{++} &= 0.023 \pm 0.009.
\end{aligned}
$$

The errors above are the combination of the statistical and systematic errors. The $\Sigma(1385)^+$ rate has been assumed to be half of the $\Sigma(1385)^\pm$ rate from [1]. JETSET, with its default parameters, has a strangeness suppression factor of 0.3 and a suppression factor of 0.4 for diquarks containing strange quarks, resulting in predictions of 0.206, 0.029, and 0.004 for these ratios. The HERWIG predictions for the above ratios are 0.373, 0.089, and 0.024 respectively. Both JETSET and HERWIG predict a $\Sigma(1385)^+$ rate that is too large and hence the ratios involving the $\Sigma(1385)^+$ disagree with the measurement. If the assumption of one single strangeness suppression factor, Λ, is made then the above ratios should be Λ, Λ^2 and Λ^3, and thus predict a factor of 0.18 ± 0.03. However the χ^2 probability for this is much less than 1%, indicating that one strangeness suppression factor is not appropriate in this decuplet.

It is now possible to extract the direct proton production rate from the measured inclusive rate using the measurements of the production rates of Λ (0.351 ± 0.019) [1], Σ^+ (0.085 ± 0.031) [3] and this measurement of Δ^{++} production, since these rates encompass most states that decay to protons. Using the OPAL measurement of the proton production rate of 0.92 ± 0.11 [2], we obtain a direct proton production rate of:

$$0.21 \pm 0.16.$$

9

While this calculation neglects charmed and bottom hadrons as well as orbitally excited N* states that could decay directly to protons, JETSET predicts that these decays contribute less than 5% of the total proton rate. It was also assumed that all the Δ states have the same production rate. The error is dominated by the uncertainties in inclusive proton and Δ^{++} rates. Due to this large error, this direct proton production rate is consistent with both no direct production and with the approximately 20% direct production predicted by the thermodynamic model of [15]. As a comparison, JETSET predicts 0.49 and HERWIG predicts 0.21.

Making the assumption that all Δ^{++} production is direct, which JETSET predicts neglects less than 0.1% of the total rate, we can give the ratio of the direct production rates of the $J^P = \frac{3}{2}^+$ Δ^{++} (baryon decuplet), to that of the $J^P = \frac{1}{2}^+$ p (baryon octet):

$$\Delta^{++}/p = 1.0 \pm 0.5 \pm 0.9.$$

The first error is due to all sources except the Δ^{++} rate and the second is that due to the Δ^{++} rate. For this ratio JETSET and HERWIG predict 0.4 and 0.8, respectively. More precision in the proton and Δ^{++} rates is necessary to make a statement on whether the models reproduce this decuplet to octet ratio.

8   Conclusion

OPAL has made the first measurement of Δ^{++} production in hadronic Z^0 decays, thus completing the measurements of each strangeness level of the lightest $J^P = \frac{3}{2}^+$ baryon decuplet. We measure a total production rate of $0.22 \pm 0.04 \pm 0.04$ $\Delta^{++} + (\overline{\Delta})^{--}$ per hadronic Z^0 decay, where the first error is statistical and the second systematic. We also report the first measurement of the Δ^{++} fragmentation function in e$^+$e$^-$ collisions away from the $\Upsilon(1S)$ resonance and find that both JETSET and HERWIG predict a spectrum that is harder than the data.

References

[1] OPAL Collaboration, P.D. Acton *et al.*, Phys. Lett. **B 291** (1992) 503.

[2] OPAL Collaboration, R. Akers *et al.*, Z. Phys. **C 63** (1994) 181.

[3] DELPHI Collaboration, P. Abreu *et al.*, CERN-PPE/95-39.

[4] DELPHI Collaboration, P. Abreu *et al.*, CERN-PPE/95-28;
ALEPH Collaboration, D. Buskulic *et al.*, Z. Phys. **C 66** (1995) 335;
ALEPH Collaboration, D. Buskulic *et al.*, Z. Phys. **C 64** (1994) 361;
L3 Collaboration, M. Acciarri *et al.*, Phys. Lett. **B 328** (1994) 223;
DELPHI Collaboration, P. Abreu *et al.*, Phys. Lett. **B 318** (1993) 249.

[5] Particle Data Group, Phys. Rev. **D 50** (1994) 1173.

[6] ARGUS Collaboration, H. Albrecht *et al.*, Phys. Lett. **B 230** (1989) 169.

[7] OPAL Collaboration, K. Ahmet *et al.*, Nucl. Instrum. Methods **A 305** (1991) 275.

[8] M. Hauschild *et al.*, Nucl. Instrum. Methods **A 314** (1992) 74.

[9] OPAL Collaboration, G. Alexander *et al.*, Z. Phys. **C 52** (1991) 175.

[10] OPAL Collaboration, P.D. Acton *et al.*, Z. Phys. **C 61** (1994) 357.

[11] T. Sjöstrand, Comput. Phys. Commun. **39** (1986) 347;
T. Sjöstrand and M. Bengtsson, Comput. Phys. Commun. **43** (1987) 367.

[12] J. Allison *et al.*, Nucl. Instrum. Methods **A 317** (1991) 47.

[13] J.D. Jackson, Il Nuovo Cimento **34** (1964) 1644.

[14] G. Marchesini and B.R. Webber, Nucl. Phys. **B 310** (1988) 461;
G. Marchesini *et al.*, Comput. Phys. Commun. **67** (1992) 465.

[15] F. Becattini, Firenze preprint, DFF 224/03/1995.

[16] OPAL Collaboration, P.D. Acton *et al.*, Z. Phys. **C 58** (1993) 387.

[17] G.D. Lafferty and T.R. Wyatt, Nucl. Instrum. Methods **A 355** (1995) 541.

x_E	Δ^{++} selection efficiency
0.05 − 0.075	0.047 ± 0.004
0.075 − 0.1	0.028 ± 0.002
0.1 − 0.15	0.071 ± 0.002
0.15 − 0.2	0.091 ± 0.004
0.2 − 0.3	0.096 ± 0.004
0.3 − 1.0	0.109 ± 0.015

Table 1: The Δ^{++} selection efficiencies in bins of x_E.

x_E	Fitted number of Δ^{++}	χ^2 probability	χ^2 probability of fit with no Δ^{++}
0.05 − 0.075	$\left(7.5^{+2.9}_{-2.5}\right) \times 10^3$	0.26	0.06
0.075 − 0.1	$\left(6.7^{+1.8}_{-1.8}\right) \times 10^3$	0.78	0.14
0.1 − 0.15	$\left(4.6^{+1.1}_{-1.1}\right) \times 10^3$	0.08	< 0.01
0.15 − 0.2	$\left(2.7^{+1.6}_{-1.5}\right) \times 10^3$	0.80	0.70
0.2 − 0.3	$\left(2.4^{+1.3}_{-1.4}\right) \times 10^3$	0.33	0.25
0.3 − 1.0	$\left(1.5^{+0.7}_{-0.8}\right) \times 10^3$	0.64	0.63

Table 2: The fitted number of Δ^{++} in each bin of x_E, where the errors are the statistical errors from the fit. Also shown is the χ^2 probability obtained from the fit and the χ^2 probability obtained from a fit with no Δ^{++} signal.

x_E	Number of Δ^{++} with mass free	fitted mass GeV$/c^2$
0.05 − 0.075	$\left(13.3^{+4.4}_{-5.3}\right) \times 10^3$	$1.20^{+0.01}_{-0.01}$
0.075 − 0.1	$\left(6.5^{+2.0}_{-1.6}\right) \times 10^3$	$1.22^{+0.02}_{-0.02}$
0.1 − 0.15	$\left(5.6^{+1.1}_{-1.3}\right) \times 10^3$	$1.19^{+0.01}_{-0.01}$
0.15 − 0.2	$\left(2.4^{+1.7}_{-1.3}\right) \times 10^3$	$1.26^{+0.03}_{-0.05}$
0.2 − 0.3	$\left(6.5^{+1.9}_{-1.5}\right) \times 10^3$	$1.19^{+0.01}_{-0.01}$
0.3 − 1.0	$\left(1.8^{+0.8}_{-0.8}\right) \times 10^3$	$1.19^{+0.04}_{-0.02}$

Table 3: The observed number of Δ^{++} when the mass is left free in the fit. The errors are the statistical errors from the fit.

x_E	Δ^{++} per event / Δx_E		x_E JETSET (HERWIG)
0.05 – 0.075	1.9 $^{+0.7}_{-0.6}$	± 0.2	0.062 (0.062)
0.075 – 0.1	2.8 $^{+0.8}_{-0.8}$	± 0.3	0.087 (0.087)
0.1 – 0.15	0.38 $^{+0.09}_{-0.09}$	± 0.03	0.123 (0.123)
0.15 – 0.2	0.18 $^{+0.10}_{-0.10}$	± 0.01	0.174 (0.173)
0.2 – 0.3	0.073 $^{+0.040}_{-0.043}$	± 0.005	0.245 (0.245)
0.3 – 1.0	0.0060 $^{+0.0029}_{-0.0029}$	± 0.0008	0.530 (0.554)

Table 4: The measured Δ^{++} fragmentation function in bins of x_E, where the first error is statistical and the second is the systematic error. Also shown are the predicted x_E values where the fragmentation function is equal to the average in each bin for JETSET and HERWIG. In figure 4, the measured values from the data have been plotted at the JETSET predicted x_E values.

x_E	Efficiency	Vertex modelling	Fragmentation	Integration bound
0.05 – 0.075	± 0.16	± 0.12	± 0.087	± 0.054
0.075 – 0.1	± 0.19	± 0.12	± 0.14	± 0.081
0.1 – 0.15	± 0.0095	± 0.019	± 0.013	± 0.011
0.15 – 0.2	± 0.0074	± 0.0093	± 0.0016	± 0.0051
0.2 – 0.3	± 0.0033	± 0.0030	± 0.00029	± 0.0021
0.3 – 1.0	± 0.00079	± 0.00022	± 0.000028	± 0.00017

Table 5: The systematic errors on the differential rate determination, in each bin of x_E. The first column shows the error due to the uncertainties in the efficiency calculation, the second column shows the error due to uncertainty in the vertex assignment efficiency, the third column shows the error due to the fragmentation model assumed, and the fourth column shows the error due to the bounds on the integration of the fitted Δ^{++} signal. The uncertainty in the extrapolation below $x_E = 0.05$ dominates the systematic error in the overall rate determination.
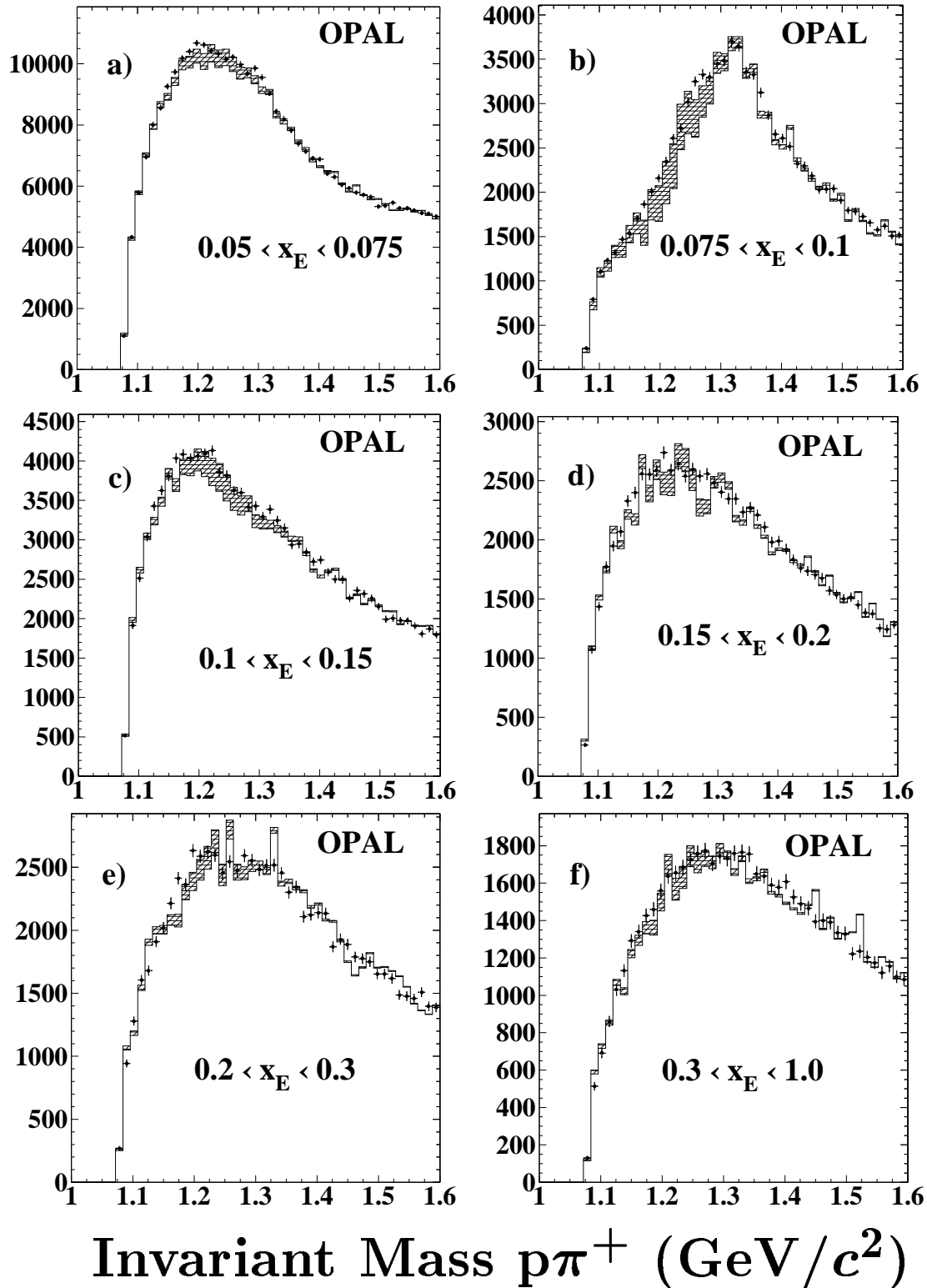
Figure 1: The Δ^{++} candidate invariant mass spectra along with the results of the fit. The open histogram is the fitted background shape and the shaded histogram shows the fitted Δ^{++} signal. The x_E bins are: a) $0.05 < x_E < 0.075$, b) $0.075 < x_E < 0.1$, c) $0.1 < x_E < 0.15$, d) $0.15 < x_E < 0.2$, e) $0.2 < x_E < 0.3$, f) $0.3 < x_E < 1.0$.
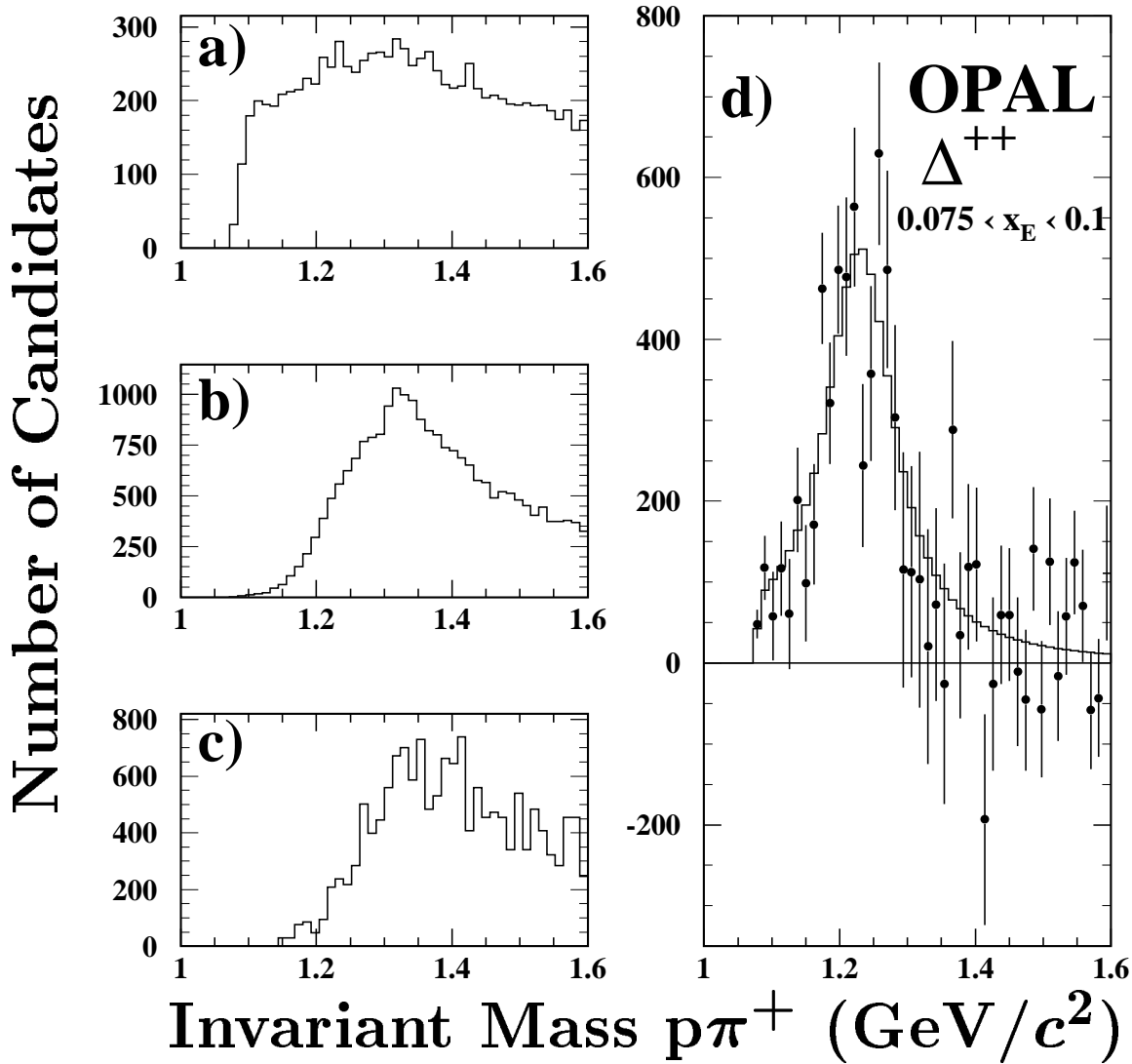
Figure 2: Some of the background shapes that make up the fit to the second x_E bin $(0.075 < x_E < 0.1)$. a) The fitted prediction for the pπ^+ component, without the Δ^{++}. b) The fitted prediction for the $\pi^+\pi^+$ component. c) The fitted prediction for the π^+p component. d) The resulting spectrum after the fitted background has been subtracted with the fitted Δ^{++} contribution shown.
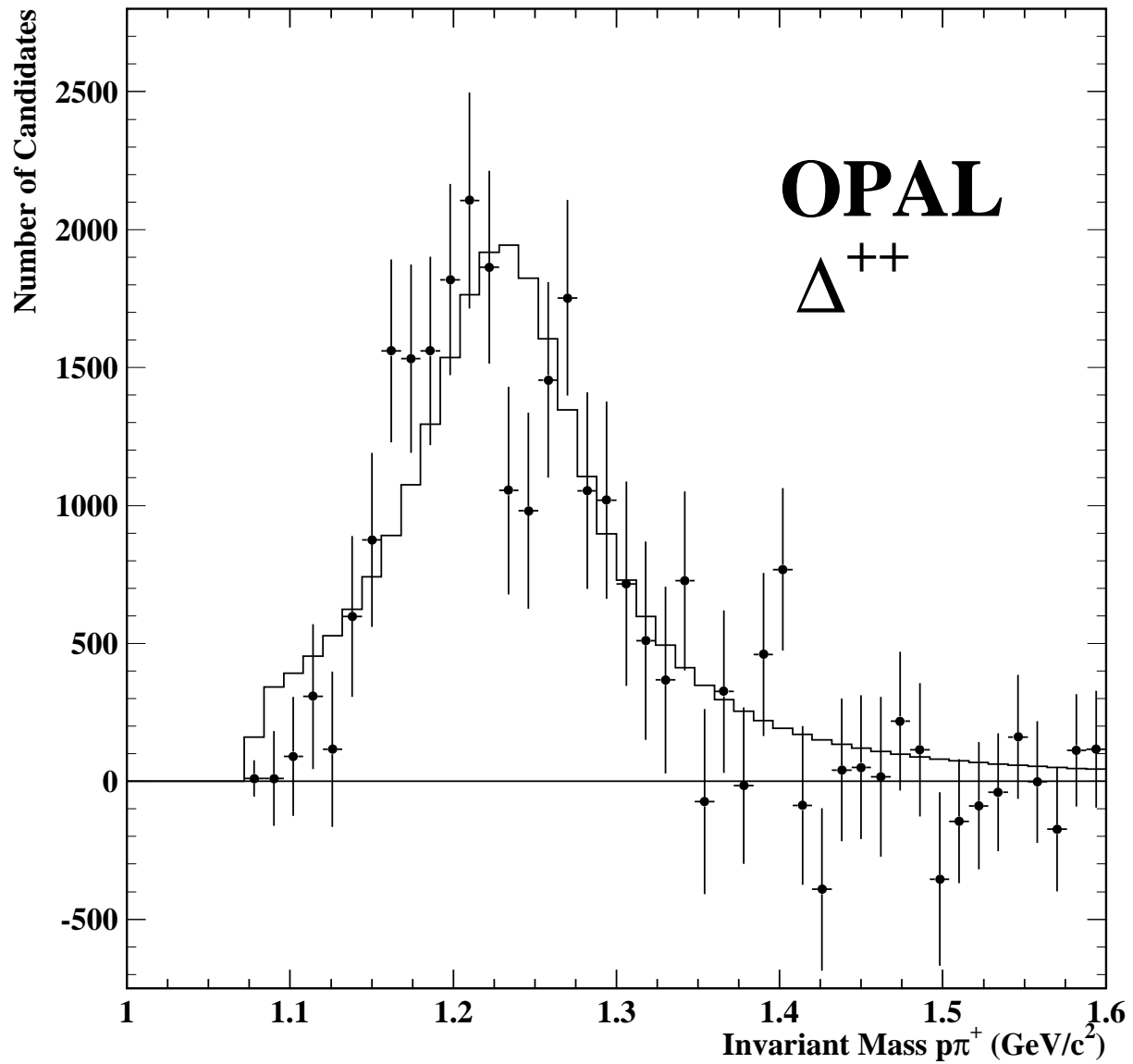
Figure 3: The Δ^{++} candidate invariant mass spectra for all bins of x_E, after subtraction of the fitted background. The line shows the fitted Δ^{++} contribution.

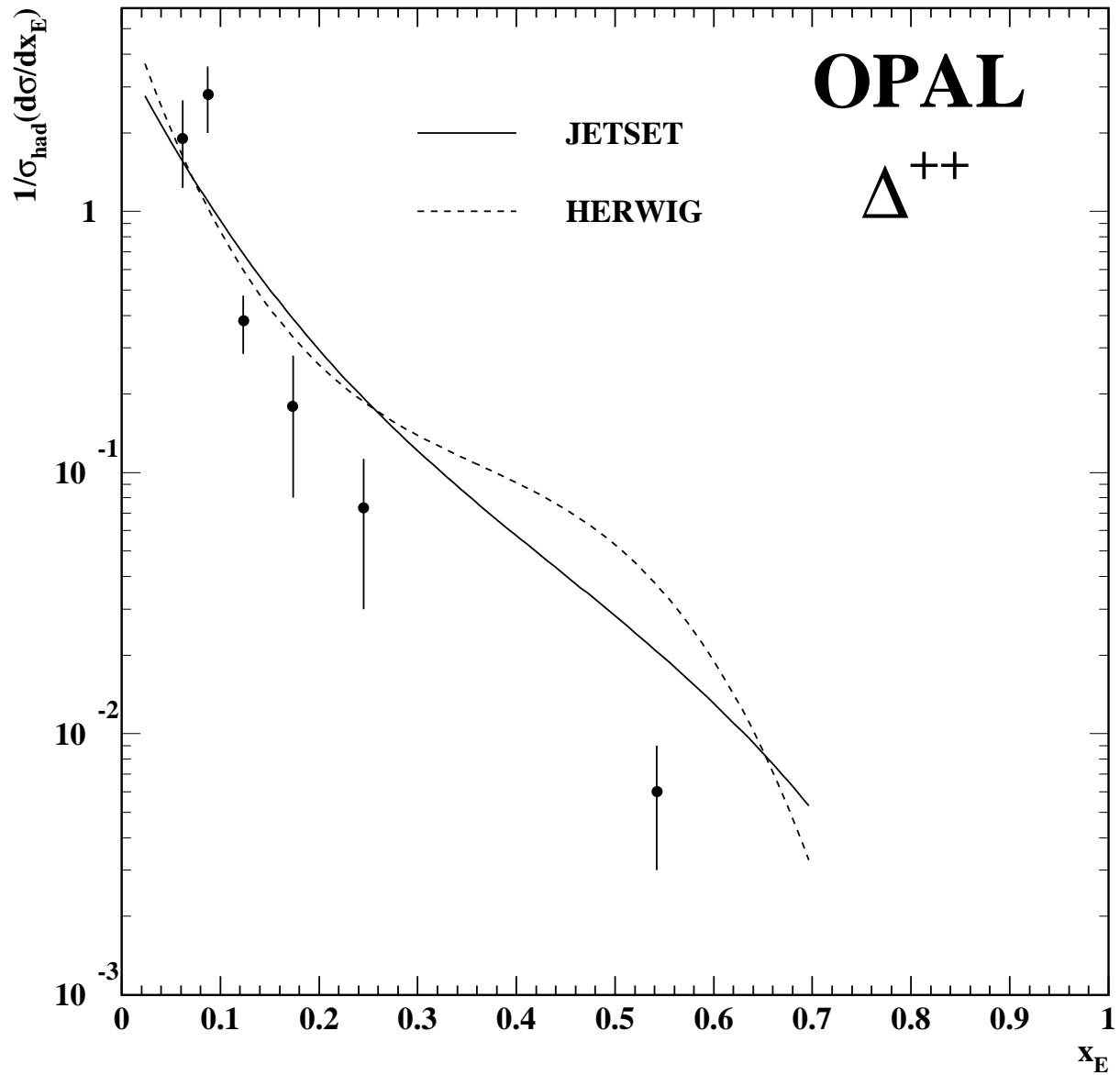Figure 4: The Δ^{++} fragmentation function as a function of x_E. The points are the measurements, the solid line is the prediction of JETSET and the dashed line is the prediction of HERWIG. The data points have been plotted at the values of x_E inferred from JETSET, given in table 4, following the prescription in [17]. The Monte Carlo predictions are normalised to the observed rates above x_E of 0.05.

18